Mesostructure Control Using a Titania-Coated Silica Nanosphere Framework with Extremely High Thermal Stability

Dong-Wook Lee,[†,‡] Son-Ki Ihm,[‡] and Kew-Ho Lee*[,†]

Membrane and Separation Research Center, Korea Research Institute of Chemical Technology, Post Office Box 107, Yuseong, Daejeon 305-606, South Korea, and Department of Chemical and Biomolecular Engineering, National Research Laboratory for Environmental Catalysis, Korea Advanced Institute of Science and Technology, 373-1 Guseong-dong, Yuseong-gu, Daejeon 305-701, South Korea

Received March 4, 2005. Revised Manuscript Received June 8, 2005

We report on a new synthetic method for mesoporous titania/silica (MTS), which is framed by titania-coated silica nanospheres. The MTS has extremely high thermal stability (stable up to 1000 °C), a high surface area (690−480 m^2/g), a high pore volume (0.65−2.16 cm^3/g), and a narrow pore size distribution. The anatase−rutile transformation of the MTS was observed at 1400 °C, which is the highest transformation temperature ever reported. We deposited titania thin film with a thickness of about 1.5 nm on surface of independent silica nanospheres (5 nm in particle diameter) via the sol−gel reaction of titanium isopropoxide in as-prepared sol of a silica nanosphere−citric acid nanocomposite. After eliminating the citric acid by calcination at 500 °C, we successfully synthesized the MTS, and by varying the concentration of the citric acid, we could precisely control the pore diameter from 3.7 nm up to 25 nm. Despite the calcination at 1000 °C, the pore diameter of the MTS was maintained with narrow pore size distribution, high surface area, and high pore volume. In addition, we successfully prepared MTS membranes that were supported on porous stainless steel. These MTS membranes have a high gas permeance and stability against water vapor. Moreover, by using MTS with various pore diameters and pore volumes, the permeance and pore diameter of the MTS membrane were easily controlled.

Introduction

Since surfactant-organized mesoporous silica was first produced in 1992,[1] much research has been reported on the synthesis of various mesoporous materials using supramolecular assembly of surfactant molecules as a template.[2−6] Recently, the approach has been extended to prepare transition-metal oxides due to their special optical, electronic, and magnetic properties.[7] As one of the most important transition-metal oxides, titania is an extremely attractive material for diverse applications such as controlled delivery, catalysts, photocatalysts, and energy conversion.[8,9] Mesoporous titania has been synthesized using a variety of templates, such as phosphates,[10,11] amines,[12−14] ions,[15−17] block polymers,[7,18,19] nonionic surfactants,[20] and nonsurfactants.[21−24] However, it is quite difficult to fabricate thermally stable mesoporous titania. The relatively low thermal stability of the titania-based mesoporous materials is often attributed to their phase transformation and pore shrinkage derived from elimination of the structure-directing agents.[25,26] Higher thermal stability was achieved only in titania, which is synthesized by poly(ethylene oxide)-based templating.[7,25,27−30] More recently, Yoshitake et al. improved the thermal stability of template

* To whom correspondence should be addressed. E-mail: khlee@krict.re.kr.
† Korea Research Institute of Chemical Technology.
‡ Korea Advanced Institute of Science and Technology.

(1) Kresge, C. T.; Leonowicz, M. E.; Roth, W. J.; Vartuli, J. C.; Beck, J. S. *Nature* **1992**, *359*, 710.
(2) Raman, N. K.; Anderson, M. T.; Brinker, C. J. *Chem. Mater.* **1996**, *8*, 1682.
(3) Sayari, A.; Liu, P. *Microporous Mater.* **1997**, *12*, 149.
(4) Barton, T. J.; Bull, L. M.; Klemperer, W, G.; Loy, D. A.; McEnaney, B.; Misono, M.; Monson, P. A.; Pez, G.; Scherer, G. W.; Vartuli, J. C.; Yaghi, O. M. *Chem. Mater.* **1999**, *11*, 2633.
(5) Ying, J. Y.; Mehnert, C. P.; Wong, M. S. *Angew. Chem., Int. Ed.* **1999**, *38*, 57.
(6) Soler-Illia, G. J. de A. A.; Sanchez, C.; Lebeau, B.; Patarin, J. *Chem. Rev.* **2002**, *102*, 4093.
(7) Yang, P. D.; Zhao, D. Y.; Margolese, D. I.; Chmelka, B. F.; Stucky, G. D. *Nature* **1998**, *396*, 152.
(8) Grosso, D.; Soler-Illia, G. J. de A. A.; Crepaldi, E. L.; Cagnol, F.; Sinturel, C.; Bourgeois, A.; B.-Bruneau, A.; Amenitsch, H.; Albouy, P. A.; Sanchez, C. *Chem. Mater.* **2003**, *15*, 4562.
(9) Hagfeldt, A.; Grätzel, M. *Chem. Rev.* **1995**, *95*, 45.
(10) Putnam, R. L.; Nakagawa, N.; Mcgrath, K. M.; Yao, N.; Aksay, I. A.; Gruner, S. M.; Navrotsky, A. *Chem. Mater.* **1997**, *9*, 2690.
(11) Stone, V. F., Jr.; Davis, R. J. *Chem. Mater.* **1998**, *10*, 1468.
(12) Antonelli, D. M. *Microporous Mesoporous Mater.* **1999**, *30*, 315.
(13) Wang, Y.; Tang, X.; Yin, L.; Huang, W.; Hacohen, Y. R.; Gedanken, A. *Adv. Mater.* **2000**, *12*, 1183.
(14) Yoshitake, H.; Sugihara, T.; Tatsumi, T. *Chem. Mater.* **2002**, *14*, 1023.
(15) On, D. T. *Langmuir* **1999**, *15*, 8561.
(16) Cabrera, S.; Haskouri, J. F.; Porter, A.-B.; Porter, D.-B.; Marcos, M. D.; Amoros, P. *Solid State Sci.* **2000**, *2*, 513.
(17) Soler-Illia, G. J. de A. A.; Louis, A.; Sanchez, C. *Chem. Mater.* **2002**, *14*, 750.
(18) Yu, J. C.; Zhang. L.; Yu, J. *Chem. Mater.* **2002**, *14*, 4647.
(19) Alberius, P. C. A.; Frindell, K. L.; Hayward, R. C.; Kramer, E. J.; Stucky, G. D.; Chmelka, B. F. *Chem. Mater.* **2002**, *14*, 3284.
(20) Kluson, P.; Kacer, P.; Cajthaml, T.; Kalaji, M. *J. Mater. Chem.* **2001**, *11*, 644.
(21) Saadoun, L.; Ayllón, J. A.; Jiménez-Becerríl, J.; Peral, J.; Domenech, X.; Rodríguez-Clemente, R. *Appl. Catal., B* **1999**, *21*, 269.
(22) Guo, C.-W.; Cao, y.; Kai, W.-L.; Fan, K.-N.; Deng, J.-F. *Chem. Lett.* **2002**, 588.
(23) Zhang, Y.; Weidenkaff, A.; Reller, A. *Mater. Lett.* **2002**, *54*, 375.
(24) Zheng, J.-Y.; Pang, J.-B.; Qiu, K.-Y.; Wei, Y. *Microporous Mesoporous Mater.* **2001**, *49*, 189.
(25) Smarsly, B.; Grosso, D.; Brezesinski, T.; Pinna, N.; Boissière, C.; Antonietti, M.; Sanchez, C. *Chem. Mater.* **2004**, *16*, 2948.
(26) Cassiers, K.; Linssen, T.; Mathieu, M.; Bai, Y. Q.; Zhu, H. Y.; Cool, P.; Vansant, E. F. *J. Phys. Chem. B* **2004**, *108*, 3713.
(27) Yang, P.; Zhao, D.; Margolese D. I.; Chmelka B. F.; Stucky, G. D. *Chem. Mater.* **1999**, *11*, 2813.

10.1021/cm050485w CCC: $30.25
Published on Web 07/26/2005

(primary amine)-extracted titania through CVD treatment of titanium isopropoxide.[14] Cassiers et al. synthesized NH_3-treated titania, which is stable up to 600 °C.[26]

One of complementing solutions for the problem of thermal stability is deposition of titania on high surface area solids such as mesoporous silicates. Bulk titania is thermally unstable and readily loses its surface area due to easy sintering at high temperature. In contrast, titania/silica materials have higher thermal stability, surface acidity, and mechanical properties than bulk titania.[31−33] In addition, the thermal expansion coefficient of these oxides does not change to a significant extent over a wide temperature range.[34] Titania was mostly deposited on high surface area materials via grafting[35−37] or the solution sol−gel method.[38,39] Recently, Aronson et al. synthesized titanium-grafted MCM-41 and FSM-16 by reacting $TiCl_4$ in hexanes with as-synthesized silicate powder, in which surfactant remained.[40] Luan and co-workers used incipient-wetness impregnation for incorporation of titanium into the mesoporous silica molecular sieve SBA-15.[41]

In this study, we deposited titania thin film on silica nanospheres via the sol−gel reaction of titanium isopropoxide in a nanocomposite sol of silica nanospheres and citric acid. After eliminating the citric acid by thermal treatment, we successfully synthesized mesoporous titania/silica (MTS) with a high surface area, a high pore volume, and extremely high thermal stability. Nitrogen adsorption, X-ray diffraction (XRD), transmission electron microscopy (TEM), and Fourier transform infrared (FTIR) spectroscopy have been used to characterize the MTS. In addition, the MTS was used to fabricate mesoporous composite membranes, which have a high permeability and stability against water vapor.

Experimental Section

Synthesis of Mesoporous Titania/Silica. Transparent colloidal silica sol was synthesized under base-catalyzed condition at the $TEOS:NH_3:H_2O:EtOH$ molar ratio of 1:0.086:53.6:40.7. Prior to addition of a NH_3/H_2O mixture, a TEOS/ethanol mixture was stirred vigorously at 50 °C. The addition of the NH_3/H_2O mixture was carried out dropwise. The final mixture was refluxed at 50 °C for 3 h, resulting in a stable colloidal silica sol, which includes silica nanospheres (SN) of about 5 nm in particle diameter. Subsequently, various concentrations of citric acid (CA) as a templating agent were added to the as-prepared colloidal silica sol and the mixture was stirred vigorously at room temperature for 10 min to obtain the SN−CA nanocomposite sol.

The nanocomposite sol of titania-coated silica nanosphere (TSN) and CA was prepared by the sol−gel reaction of titanium isopropoxide (TIP) in the as-prepared SN−CA sol. A 0.06 M concentration of TIP was dropped carefully into the SN−CA sol and stirred vigorously at 90 °C for 60 min, followed by addition of hydrochloric acid (HCl) to adjust the pH of the solution close to 1. After the final mixture was refluxed with vigorous stirring at 90 °C for 12 h, the TSN−CA nanocomposite sol was obtained. The TSN−CA sol was dried at 70 °C for 12 h and then calcined at 500 °C. After eliminating the CA via thermal treatment, we successfully synthesized mesoporous titania/silica, which is framed by the TSN (about 8 nm in particle diameter). The mesoporous titania/silica is designated as MTS(x), where x is the Si/CA molar ratio in the TSN−CA nanocomposite sol. For the purpose of comparison, mesoporous silica (MS), which is framed by 5 nm SNs, was also synthesized after eliminating the CA from the SN−CA nanocomposite by calcination at 500 °C.

Characterization. To characterize the MTS, we used nitrogen adsorption, X-ray diffraction (XRD), transmission electron microscopy (TEM), and Fourier transform infrared (FTIR) spectroscopy. Nitrogen adsorption/desorption isotherms of the MTS and the MS were taken by a Micromeritics ASAP 2020 instrument. Pore size distribution curves were obtained from the desorption branch by using the Barrett−Joyner−Halenda (BJH) method. The XRD patterns were collected on a Rigaku D/MAX-2200V instrument operated at 1.6 kW. TEM analysis was carried out on a JEOL FE-TEM, JEM-2100F, operated at 200 kV. FTIR spectra were taken on Bio Rad Digilab Division FTS-165 FTIR. To confirm the titania thin film coated on the SN surface, we aged the MTS in NH_3 solution (pH = 10) for 5 days and investigated the difference in pore properties of the MTS between before and after aging in the alkaline solution.

Synthesis of Mesoporous Composite Membranes. As a substrate of a composite membrane, we used disks of 316L porous stainless steel (SUS) with a surface area of 5 cm^2, which were purchased from Matt Metallurgical. To make the substrate surface smooth, the silica xerogels (100 nm in particle size) were pressed into the macropores of one side of the SUS substrate by using a press under 10 MPa, followed by calcination at 650 °C. The SN−CA and the TSN−CA sols were used to coat the mesoporous top layers of the MS and MTS on the substrates, respectively. The mesoporous MS and MTS membranes were successfully prepared via the soaking-rolling method suggested by Lee et al.,[42] followed by calcination at 500 °C. To investigate stability of the MTS composite membranes against water vapor, we conducted a water vapor permeation test with He carrier gas at 200 °C. Before and after the vapor permeation test, we also conducted a permeation test with a H_2 (50%)/N_2 (50%) gaseous mixture.

Results and Discussion

We report on a new synthetic method of mesoporous titania/silica (MTS), which is framed by titania-coated silica nanospheres (TSN). The MTS has extremely high thermal stability (stable up to 1000 °C), a high specific surface area, a high pore volume, and a narrow pore size distribution. The

(28) Grosso, D.; Soler-Illia, G. J. de A. A.; Babonneau, F.; Sanchez, C.; Albouy, P.-A.; B.-Bruneau, A.; Balkenade, A. R. *Adv. Mater.* **2001**, *13*, 1085.
(29) Crepaldi, E. L.; Soler-Illia, G. J. d. A. A.; Grosso, D.; Sanchez, C. *New J. Chem.* **2003**, *27*, 9.
(30) Yu, J.; Yu, J. C.; Ho, W.; Jiang, Z. *New J. Chem.* **2002**, *26*, 607.
(31) Guo, X.-C.; Dong, P. *Langmuir* **1999**, *15*, 5535.
(32) Schrijnemakers, K.; Impens, N. R. E. N.; Vansant, E. F. *Langmuir* **1999**, *15*, 5807.
(33) Khalil, K. M. S.; Elsamahy, A. A.; Elanany, M. S. *J. Colloid Interface Sci.* **2002**, *249*, 359.
(34) Mariscal, R.; Granados, M.-L.; Fierro, J. L. G.; Sotelo, J. L.; Martos, C.; Grieken, R. V. *Langmuir* **2000**, *16*, 9460.
(35) Hanprasopwattana, A.; Srinivasan, S.; Sault, A. G.; Datye, A. K. *Langmuir* **1996**, *12*, 3173.
(36) Fereres, M.-G.; Alemany, L. J.; Mariscal, R.; Bañares, M. A.; Anderson, J. A.; Fierro, J. L. G. *Chem. Mater.* **1995**, *7*, 1342.
(37) Maschmeyer, T.; Rey, F.; Sankar, G.; Thomas, J. M. *Nature* **1995**, *378*, 159.
(38) Tanev, P. T.; Chibwe, M.; Pinnavaia, T. J. *Nature* **1994**, *368*, 321.
(39) Liu, Z.; Davis, R. J. *J. Phys. Chem.* **1994**, *98*, 1253.
(40) Aronson, B. J.; Blanford, C. F.; Stein A. *Chem. Mater.* **1997**, *9*, 2842.
(41) Luan, Z.; Maes, E. M.; van der Heide, P. A. W.; Zhao, D.; Czernuszewicz, R. S.; Kevan, L. *Chem. Mater.* **1999**, *11*, 3680.
(42) Lee, D.-W.; Nam, S.-E.; Sea, B. K.; Ihm, S.-K.; Lee, K.-H. *J. Membr. Sci.* **2004**, *243*, 243.

pore diameter of the MTS was exactly controlled by varying the concentration of the citric acid (CA) in TSN−CA nanocomposite sol. For comparison, we also synthesized mesoporous silica (MS), which is framed by 5 nm silica nanospheres (SN), by calcination at 500 °C to eliminate the CA from the SN−CA nanocomposite. Changes in the pore size distribution of the MTS were observed at various CA concentrations. Figure 1a shows the pore size distributions of the MS(x) and MTS(x) calcined at 500 °C in air, where x is the Si/CA molar ratio in the SN−CA and TSN−CA nanocomposites. The distributions are calculated from desorption branch of the nitrogen sorption isotherm by using the BJH method. The MS(5.85) and MTS(5.85) show average pore diameters of 2.7 and 3.7 nm with very narrow pore size distribution, respectively. Table 1 presents the pore properties of the MS and the MTS. While the BET surface area and the total pore volume of the MTS(5.85) were 690 m^2/g and 0.65 cm^3/g, those of the MS(5.85) were 790 m^2/g and 0.56 cm^3/g, respectively. The pore diameter of the MTS is about 1 nm larger than that of the MS, although the titania deposition on the wall of the silica framework is expected to result in pore narrowing. Compared with the MS(5.85), the MTS(5.85) had a decreased surface area and an increased pore volume. An increase in the pore diameter decreases the surface area at a fixed pore volume, whereas an increase in the pore volume increases the surface area at a fixed pore size.[45] Therefore, considering the decrease in the surface area of the MTS(5.85), it can be inferred that the increase in the pore size dominantly affects the specific surface area of the MTS. The sharp monomodal distribution of the MTS(5.85), which is similar to that of the MS(5.85), means in part that the titania thin film was uniformly deposited on the 5 nm SNs without second-phase titania particles or aggregates.

As the Si/CA molar ratio in the TSN−CA nanocomposite sol decreased from 5.85 to 0.09, the average pore diameter of the MTS(x) increased from 3.7 nm up to 25 nm with a sharp pore size distribution. As shown in Table 1, the pore volume of the MTS(x) increased from 0.65 to 2.16 cm^3/g and the BET surface area decreased from 690 to 480 m^2/g with the increase in the concentration of the CA as a templating agent. The large pore diameter of 25 nm with the sharp pore size distribution clearly implies that the TSN frameworks have a high thermal stability. Figure 1b shows N_2 adsorption/desorption isotherms of the MTS(x) calcined at 500 °C. All of the samples give typical type IV isotherms with a H2 hysteresis loop, which is commonly associated with ink-bottle pores or voids between close-packed spherical particles. When the Si/CA molar ratio increased, the pore volume increased and the sharp inflection of the hysteresis loop shifted toward higher P/P_o values, indicating that the pore diameter of the MTS increased.

Figures 1c and 2 show the pore size distributions and XRD patterns of the MTS(4.27) after calcination at temperatures ranging from 500 to 1400 °C, respectively. The pore size

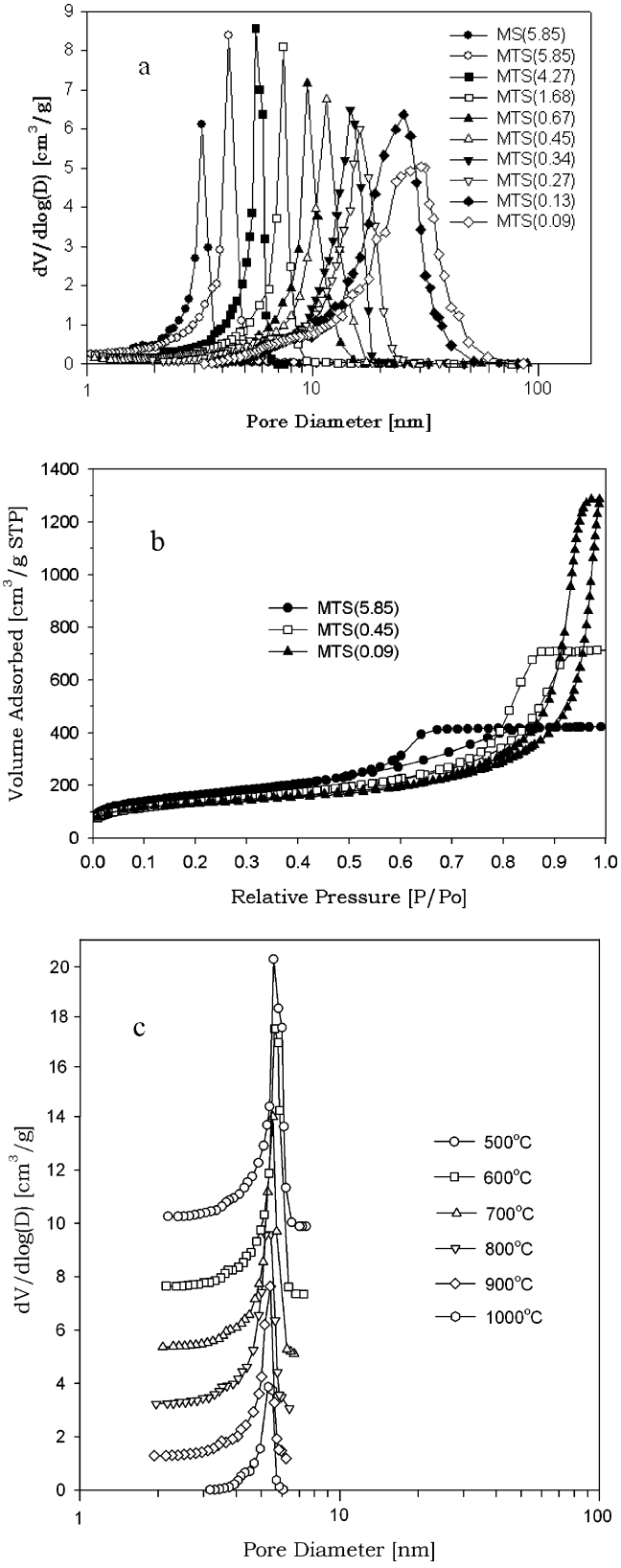

Figure 1. (a) Pore size distributions of MS(x) and MTS(x) calcined at 500 °C in air, where x is the Si/CA molar ratio in the SN−CA and TSN−CA nanocomposites. (b) N_2 adsorption/desorption isotherms of MTS(x) calcined at 500 °C. (c) Pore size distributions of the MTS(4.27) after thermal treatment in temperature range of 500−1000 °C.

distribution of the MTS(4.27) did not shift its maximum of 5.1 nm, despite the thermal treatment at 1000 °C. As shown in Table 1, the pore volume decreased from 0.76 to 0.55

(43) Takahashi, R.; Sato, S.; Sodesawa, T.; Kawakita, M.; Ogura, K. *J. Phys. Chem. B* **2000**, *104*, 12184.
(44) Lee, D.-W.; Ihm, S.-K.; Lee, K.-H. *Microporous Mesoporous Mater.* **2005**, in press.
(45) Pang, J. B.; Qiu, K. Y.; Wei, Y. *J. Non-Cryst. Solids* **2001**, *283*, 101.

Table 1. Pore and Pore Wall Properties of MS and MTS Obtained from Nitrogen Sorption and XRD Results

sample	calcinatn temp (°C)	cryst phase of the pore wall	S_{BET}[a] (m^2/g)	V[b] (cm^3/g)	anatase cryst size [c](nm)
MS(5.85)	500	amorphous	790	0.56	
MTS(5.85)	500	anatase	690	0.65	NM[d]
MTS(4.27)	500	anatase	660	0.76	9.1
MTS(0.45)	500	anatase	580	1.10	NM
MTS(0.27)	500	anatase	500	1.35	NM
MTS(0.09)	500	anatase	480	2.16	NM
MTS(4.27)	600	anatase	650	0.75	9.3
MTS(4.27)	700	anatase	610	0.70	9.8
MTS(4.27)	800	anatase	520	0.60	10.6
MTS(4.27)	900	anatase	490	0.55	11.2
MTS(4.27)	1000	anatase	280	0.30	13.3
MTS(4.27)	1300	anatase	80	0.15	25.5
MTS(4.27)	1400	anatase−rutile−crystobalite	30	0.10	27.8

[a] BET surface area. [b] Total pore volume taken from the volume of N_2 adsorbed at $P/P_o = 0.995$. [c] Calculated from the (1,0,1) peak of anatase phase using the Scherrer equation. [d] Not measured.

cm^3/g, and the surface area decreased from 660 to 490 m^2/g with the increase in the calcination temperature from 500 to 900 °C. At 1000 °C, the pore volume and the surface area rapidly decreased to 0.3 cm^3/g and 280 m^2/g, though they remained high. In the XRD patterns of the MTS(4.27) calcined in temperature range 500−1000 °C, diffraction peaks of the anatase titania were detected along with a broad band, which is attributed to the amorphous SN. The relatively low intensity and large fwhm of the anatase peaks indicate that the titania was well-deposited on the SNs in the absence of second-phase titania particles. A significant change in the intensity and the fwhm of the peaks was not observed with increasing calcination temperature until 1000 °C, which implies there was no substantial growth of the anatase crystallites. However, calcination of the MTS at 1300 °C led to a decrease in the fwhm of the peaks assigned to anatase because the sintering at extremely high temperature caused the growth of anatase crystal. After calcination of the MTS at 1400 °C, weak diffraction peaks of the rutile phase were observed with crystallization of the crystobalite.

Table 1 also shows that the size of the anatase crystal in the MTS(4.27), which is calculated from the Scherrer equation, was not significantly increased until 1000 °C. While the anatase is generally transformed into a rutile by thermal treatment in the temperature range 700−1200 °C, we observed an anatase−rutile transformation of the MTS after calcination at 1400 °C, which is the highest transformation temperature ever reported.[46,47] Because the 5 nm SN cores, which proved thermally stable in our previous study,[44] maintained the large distance between the anatase clusters deposited on the SNs, the anatase−rutile phase transformation was suppressed below 1400 °C. In other words, a lower coordination of the primary anatase clusters reduces the chance of a rutile nucleus reaching the critical size.[46] Moreover, as an additive, silica inhibits the anatase−rutile transformation.[48] It is well-known that the relatively low

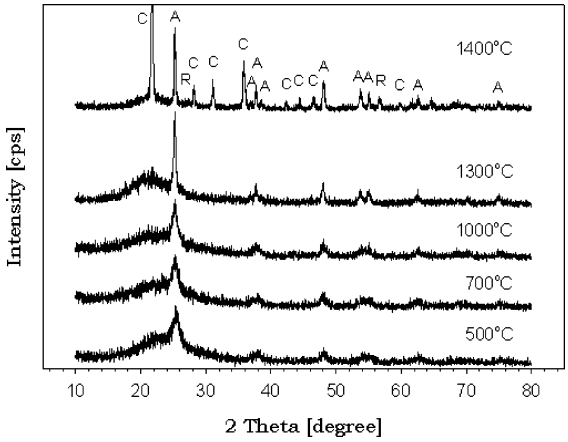

Figure 2. XRD patterns of the MTS(4.27) prepared at calcination temperatures ranging from 500 to 1400 °C (A, anatase; R, rutile; C, crystobalite). The anatase−rutile phase transformation was observed after calcination at 1400 °C.

thermal stability of mesoporous titania is often attributed to the crystallization of titania.[49] The grain growth of titania nanocrystallites via sintering, with an extensive loss of surface area, can be enhanced during the phase transformation of anatase to rutile.[50] In the case of the MTS, the anatase phase was significantly stable up to 1300 °C without the anatase−rutile transformation, as evident from Table 1 and Figures 1c and 2. We deduce, therefore, that the high thermal stability of the MTS is attributed to the stable anatase phase. In addition, the highly dense structure of the SN cores with a particle size of about 5 nm contribute to the extremely high thermal stability of the MTS, because the thicker pore wall can improve the thermal and hydrothermal stability of mesoporous materials.[51]

Figure 3a,b exhibits TEM images of the MS(4.27) and MTS(4.27) calcined at 500 °C. The MS(4.27) and MTS-(4.27) show wormholelike mesostructure, and the mesopores are three-dimensionally disordered. The primary TSNs of the MTS in Figure 3b have a particle size of around 8 nm, which is larger than the primary SNs (5 nm) of the MS in Figure 3a. The particle size of the primary TSN is almost consistent with the size of the anatase crystal, which was calculated from the Scherrer equation in Table 1. The relatively uniform size of the independent TSNs leads to the narrow monomodal distribution of the MTS pore diameter as shown in Figure 1a. A high-magnification TEM image of the MTS(4.27) in Figure 3c shows the presence of anatase nanocrystals (approximately 8 nm in diameter) with clearly resolved lattice fringes, which indicates that the anatase−titania film of around 1.5 nm in thickness was successfully deposited on the 5 nm SNs. As a result, if a titania monolayer is assumed to have a thickness of 0.355 nm (the interlayer spacing for the {101} plane of the anatase structure of titania),[31] it can be inferred that about 4 monolayers of anatase−titania were coated on the 5 nm SNs. The electron diffraction pattern of the selected area exhibits several

(46) Yang, J.; Ferreira, J. M. F. *Mater. Lett.* **1998**, *36*, 320.
(47) Ocaña, M.; G.-Ramos, J. V.; Serna, C. J. *J. Am. Ceram. Soc.* **1992**, *75*, 2010.
(48) Kumar, K.-N. P.; Kumar, J.; Keizer, K. *J. Am. Ceram. Soc.* **1994**, *77*, 1396.
(49) Crepaldi, E. L.; Soler-Illia, G. J. de A. A.; Grosso, D.; Cagnol, F.; Ribot, F.; Sanchez, C. *J. Am. Chem. Soc.* **2003**, *125*, 9770.
(50) Kumar, K.-N. P.; Keizer, K.; Burggraaf, A. J.; Okubo, T.; Nagamoto, H.; Morooka, S. *Nature* **1992**, *358*, 48.
(51) Wang, Y.-D.; Ma, C.-L.; Sun, X.-D.; Li, H.-D. *Appl. Catal., A* **2003**, *246*, 161.

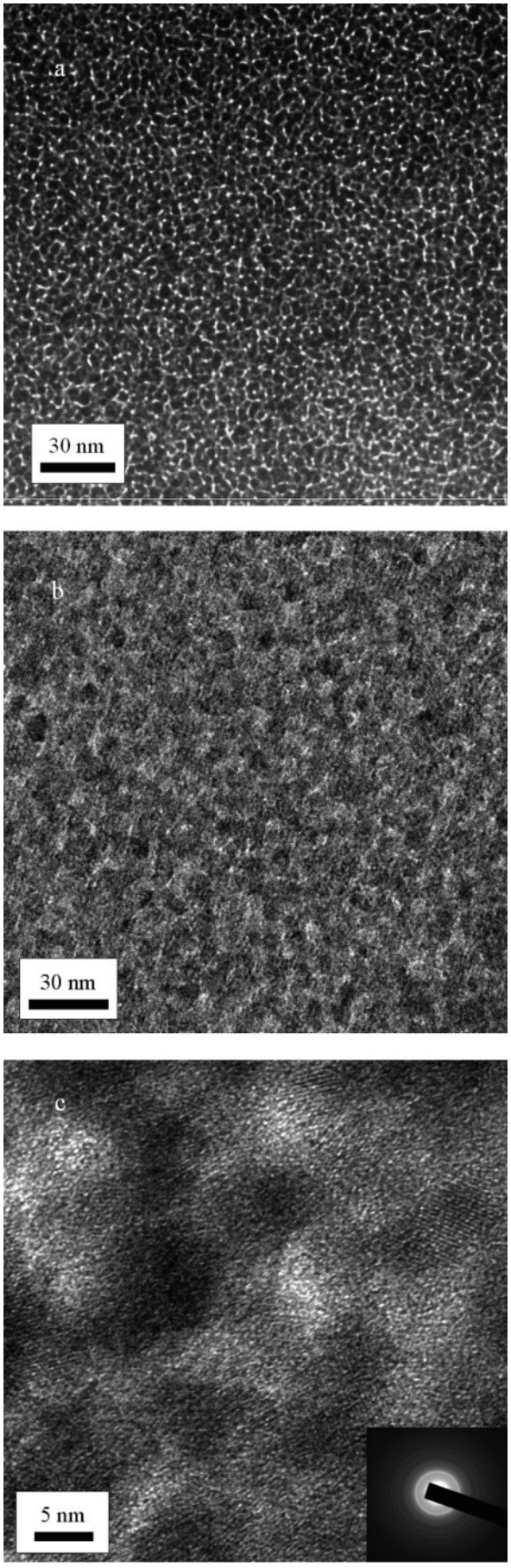

Figure 3. TEM micrographs of the MS and MTS calcined at 500 °C: (a) MS(4.27); (b) MTS(4.27); (c) a local enlarged image of part b. The inset is an electron diffraction pattern corresponding to anatase.

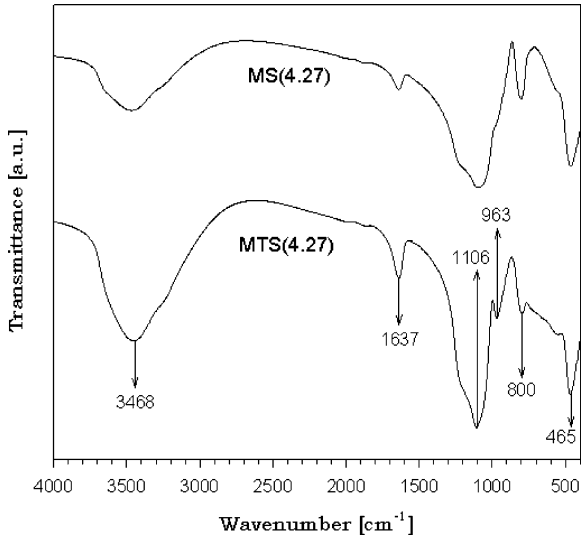

Figure 4. FTIR spectra of the MS(4.27) and MTS(4.27) calcined at 500 °C.

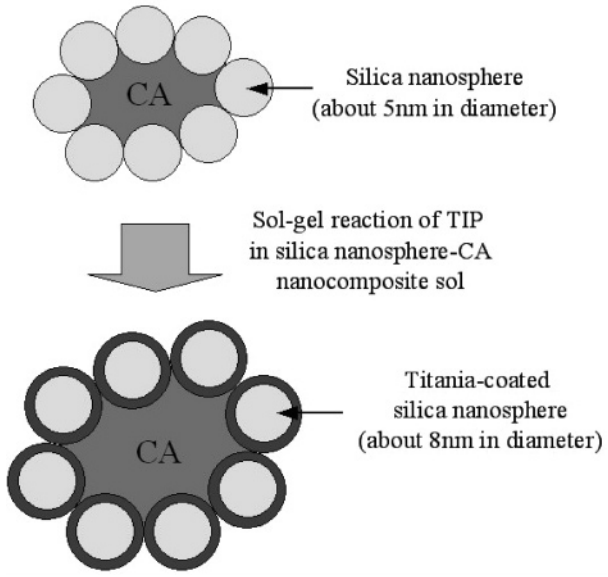

Figure 5. Schematic representation for the mechanism of the pore formation in the MTS.

diffraction rings that correspond to reflections of the anatase phase of the titania (Figure 3c, inset).

Figure 4 presents FTIR spectra of the MS(4.27) and MTS(4.27). The bands at 3468 and 1637 cm^{-1} can be attributed to the stretching vibration of the OH group and molecular H_2O, respectively. The 1106 cm^{-1} peak can be assigned to the asymmetric Si−O−Si stretching vibration, and the bands at 800 and 465 cm^{-1} can be attributed to the symmetric stretching and deformation modes of Si−O−Si, respectively. In contrast to the MS(4.27), the MTS(4.27) exhibits a band at 963 cm^{-1}, which can be assigned to the asymmetric Si−O−Ti vibration, and a broad peak at 550 cm^{-1}, which is representative of titania. The band at 963 cm^{-1} is considered to be the fingerprint of the titania deposition on the SNs. On the basis of the results in Figures 1−4, the mechanism of the pore formation in the MTS is schematically elucidated in Figure 5. The schematic diagram is in good agreement with the TEM image of the MTS shown in Figure 3c. In the as-prepared SN−CA sol, amorphous

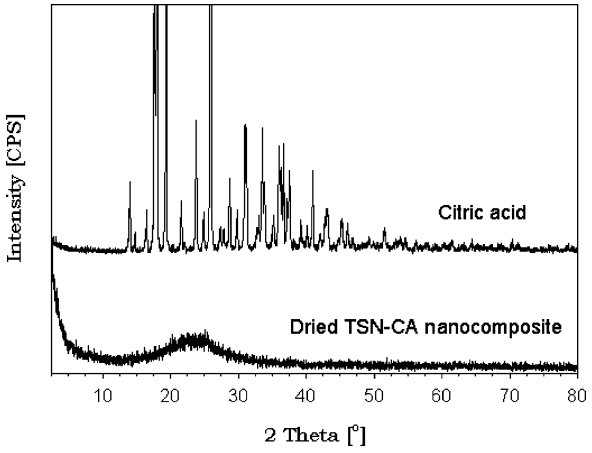

Figure 6. XRD patterns of the citric acid and the dried TSN−CA nanocomposite at 70 °C.

SN−CA nanocomposites are formed through weak hydrogen bonding between surface silanol groups of the SNs and hydroxyl groups of CA.[44] The formation of the amorphous silica−CA nanocomposite under basic condition is almost consistent with that under acidic condition reported by Takahashi et al.[43,44] After the sol−gel reaction of the TIP in the SN−CA sol, amorphous TSN−CA nanocomposites are synthesized via deposition of the titania on surface of the SNs. The formation of the amorphous TSN−CA nanocomposite was corroborated by XRD patterns of the CA and the dried TSN−CA nanocomposite at 70 °C (Figure 6). The dried TSN−CA nanocomposite shows a broad band corresponding to the amorphous silica without diffraction peaks of the CA crystal, due to the formation of the amorphous nanocomposite.

As reported in other publications, most of the titania that is supported on the mesoporous silica shows a decrease in pore size, because of the titania coating on the pore wall of the as-synthesized silica.[32,40,41] However, the pore diameter of the MTS(5.85) is about 1 nm larger than that of the MS(5.85) (Figure 1a), because the titania thin film was deposited on each primary SN (Figure 5). That is, the increase in the pore size indicates that the titania was coated on not only SN−CA interfaces (pore walls) but also SN−SN interfaces. If titania is only deposited on the SN−CA interfaces, the pore size of the MTS(5.85) will be smaller than that of the MS(5.85). Prior to drying and calcination of the SN−CA sol, which lead to Si−O−Si bonding at the SN−SN interfaces, only a little attractive interaction such as hydrogen bonding is present at the SN−SN interfaces. Si−O−Ti bonding can be formed at the SN−SN interfaces as well as the pore walls, because strength of the hydrogen bonding between the SNs is not so strong to inhibit the Si−O−Ti bonding at the SN−SN interfaces. To confirm the formation of the titania film on the SN surface, we aged the MTS in NH_3 solution (pH = 10) for 5 days and investigated the difference in pore properties of the MTS between before and after aging in the alkaline solution. Figure 7 shows variation in a pore volume and a specific surface area of the MTS(4.27) with an increase in aging time under the basic condition. Pore properties of the MTS were almost constant after aging for 5 days. These results indicate that the titania thin film was well-coated on

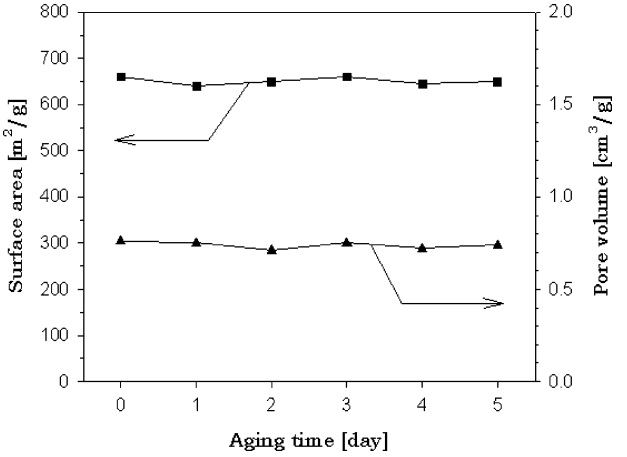

Figure 7. Variation in a pore volume and a specific surface area of the MTS(4.27) with an increase in aging time under basic condition (pH = 10).

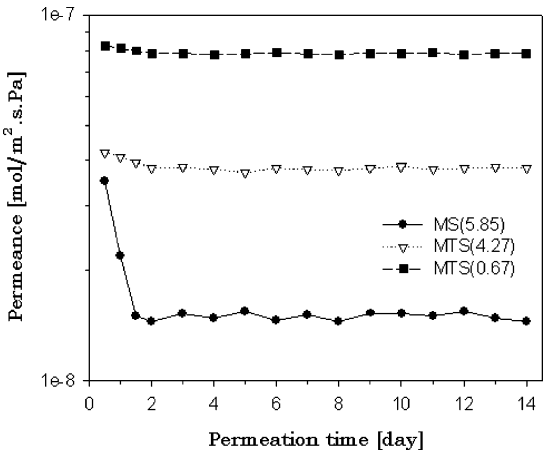

Figure 8. Results of water vapor permeation for the MS(5.85), the MTS(4.27), and the MTS(0.67) composite membranes at 200 °C for 2 weeks.

the SN surface, because silica is generally unstable under the basic condition, contrary to titania.[52,53]

The MTS is expected to be applied to various fields such as catalysis, dye-sensitized solar cells, and composite membranes. We used it to prepare porous stainless steel-supported composite membranes with high permeance and stability against water vapor. Exposure to water vapor decreases the pore properties of silica materials such as the pore volume, pore size, and uniformity, due to pore narrowing and rupture of the pore walls.[54] Silica composite membranes also show a significant falloff of gas permeance even in humid conditions.[55] To investigate the stability of the MTS composite membranes against water vapor, we conducted a water vapor permeation test with He carrier gas at 200 °C. Before and after the vapor permeation test, we also conducted a permeation test with a H_2 (50%)/N_2 (50%) gaseous mixture. As shown in Figure 8, the H_2O permeances of the MTS membranes are nearly constant with the permeation time,

(52) Silva, C. R.; Airoldi, C.; Collins, K. E.; Collins, C. H. *J. Chromatogr., A* **2005**, *1073*, 155.
(53) Fonseca, D. A.; Collins, K. E.; Collins, C. H. *J. Chromatogr., A* **2004**, *1030*, 209.
(54) Carrott, M. M. L. R.; Candeias, A. J. E.; Carrott, P. J. M.; Unger, K. K. *Langmuir* **1999**, *15*, 8895.
(55) Asaeda, M.; Yamasaki, S. *Sep. Purif. Technol.* **2001**, *25*, 151.

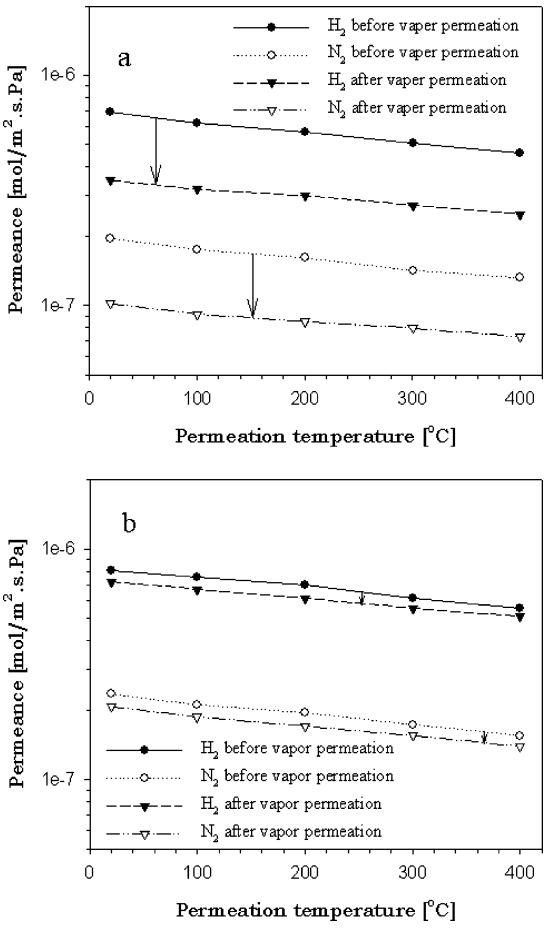

Figure 9. Permeation results of (a) MS(5.85) and (b) MTS(4.27) composite membranes with a H_2 (50%)/N_2 (50%) gaseous mixture, before and after the water vapor permeation for 2 weeks.

except a slight decrease for 2 days. Moreover, as a result of the larger pore size and pore volume of the MTS(0.67), the H_2O permeance of the MTS(0.67) membrane is much higher than that of the MTS(4.27) membrane. In contrast, the MS(5.85) membrane showed a significant decrease in the H_2O permeance after 2 days. As shown in Figure 9, the MTS(4.27) membrane showed a slight difference in the H_2 and N_2 permeances between before and after the vapor permeation. The H_2/N_2 selectivity of the MTS(4.27) membrane is about 3.5, which approaches 3.74 of an ideal H_2/N_2 selectivity for Knudsen diffusion mechanism. On the other hand, the gas permeances of the MS(5.85) membrane considerably decreased after the vapor permeation for 2 weeks. Considering the low stability of silica materials against water vapor, the deposition of the titania film on the SN surface can be clearly corroborated by the results shown in Figures 8 and 9. The titania thin film on the silica framework is a barrier that prevents water vapor from penetrating the silica matrix, resulting in enhancement of the stability against water vapor. Another notable feature of the results is that we can easily synthesize various composite membranes with different pore sizes by using the MTS.

Conclusions

We successfully synthesized mesoporous titania/silica (MTS) from a TSN−CA nanocomposite sol. The MTS has extremely high thermal stability (stable up to 1000 °C), a high specific surface area (690−480 m^2/g), a high pore volume (0.65−2.16 cm^3/g), and a narrow pore size distribution. Titania thin film of about 1.5 nm in thickness can be deposited on the surface of primary SNs without second-phase titania particles or aggregates via the sol−gel reaction of TIP in the as-prepared SN−CA nanocomposite sol, resulting in the formation of the TSN−CA nanocomposite. After calcination of the TSN−CA nanocomposite at 500 °C, the MTS was successfully synthesized, and its pore size was exactly tuned from 3.7 nm up to 25 nm by varying the CA concentration. Despite calcination at 1000 °C, the pore diameter of the MTS was maintained with a narrow pore size distribution and a relatively high surface area (280 m^2/g) and pore volume (0.3 cm^3/g). After calcination of the MTS at 1400 °C, we observed the anatase−rutile transformation and crystallization of the crystobalite. The stable anatase phase and densely structured SN cores led to the remarkable thermal stability of the MTS. In addition, we used the MTS to prepare porous stainless steel-supported MTS membranes with high gas permeance and stability against water vapor. The titania thin film on the silica framework is a barrier that prevents the water vapor from penetrating the silica matrix, resulting in enhancement of the stability against water vapor.

CM050485W